

RSC Applied Polymers

Accepted Manuscript

This article can be cited before page numbers have been issued, to do this please use: Z. Luo, X. Li and L. A. Fielding, *RSC Appl. Polym.*, 2025, DOI: 10.1039/D5LP00232J.



This is an Accepted Manuscript, which has been through the Royal Society of Chemistry peer review process and has been accepted for publication.

Accepted Manuscripts are published online shortly after acceptance, before technical editing, formatting and proof reading. Using this free service, authors can make their results available to the community, in citable form, before we publish the edited article. We will replace this Accepted Manuscript with the edited and formatted Advance Article as soon as it is available.

You can find more information about Accepted Manuscripts in the <u>Information for Authors</u>.

Please note that technical editing may introduce minor changes to the text and/or graphics, which may alter content. The journal's standard Terms & Conditions and the Ethical guidelines still apply. In no event shall the Royal Society of Chemistry be held responsible for any errors or omissions in this Accepted Manuscript or any consequences arising from the use of any information it contains.



View Article Online

View Journal

Enhancement of high concentration aqueous iron oxide nanoparticle ink printability through well-defined polymer additives

Zhidong Luo, a,b, c Xueyuan Li, a,b and Lee A. Fielding *a,b

- a. Department of Materials, School of Natural Sciences, University of Manchester, Oxford Road, Manchester M13 9PL, U.K.
- b. Henry Royce Institute, The University of Manchester, Oxford Road, Manchester M13 9PL, U.K.
- c. School of Engineering, The University of Liverpool, Liverpool L69 3BX, U.K.

Abstract. Polymer additives play a crucial role in modifying the stability and rheology of ceramic nanoparticle suspensions. A library of anionic, cationic and non-ionic polymer additives were prepared *via* reversible addition-fragmentation chain transfer (RAFT) solution polymerisation and the impact of these polymer additives on the stability, rheology and printability of aqueous iron oxide nanoparticle (IOP) suspensions was investigated. Zeta potential measurements, particle size characterisation and sedimentation experiments at a range of pH values revealed that the polymer additives significantly altered IOP suspension stability. Specifically, poly(glycerol monomethacrylate) (PGMA), quatenised poly(2-(dimethylamino)ethyl methacrylate) (q-PDMAEMA), poly(2-(dimethylamino)ethyl methacrylate) (PDMAEMA), and polyethyleneimine (PEI) enhanced stability in acidic conditions. At neutral and alkaline pH, the stability was significantly improved with the addition of poly(methacrylic acid) (PMAA) and PGMA. Subsequently, rheological assessments on IOP suspensions with 0.5% w/w of polymer additive demonstrated that PGMA48 reduced the dispersion viscosity at all pHs studied. In contrast, PDMAEMA48 and PEI reduced the viscosity at pH 3 but increased it at pH 7 and 10. Poly(potassium 3-sulfopropyl methacrylate) (PKSPMA49) consistently raised the viscosity at all pH values studied. The practical application of these findings was demonstrated through the direct ink writing (DIW) of polymer additive-containing IOP inks to form 11-layered thin-walled square structures, which showed enhanced shape retention and crack-free drying on aluminium substrates. These findings underscore the potential of precise polymer additives to refine ceramic ink rheology at minimal polymer loadings, paving the way for the development of tailored polymer additives for ceramic ink formulation and 3D printing technologies.

Introduction

Iron oxide nanoparticles (IOPs), known for their soft magnetic properties and high surface area, are extensively employed in various applications including water treatment, 1,2 diagnostic imaging,^{3,4} drug delivery,^{4,5} and inductive structures.^{6–8} However, the machining of IOP-based ceramics into complex structures presents significant challenges due to their inherent hardness and brittleness.9-12 Traditional ceramic manufacturing techniques, such as tape casting,13 gel casting,14,15 slip casting,16,17 and injection molding, 18,19 facilitate the creation of intricate designs. However, these methods are prone to defects in the demoulding stage, which is critical for producing structures with thin walls, high aspect ratios, or intricate cornering. As an innovative solution, additive manufacturing (AM) has emerged as a potential alternative. This technology builds near-net-shape objects layerby-layer directly from three-dimensional (3D) model data, eliminating the need for moulds.9,10,20,21 These attributes of AM make it an exceptionally promising approach for overcoming the manufacturing challenges associated with crafting ceramic items.

Extrusion-based direct ink writing (DIW), a sub-branch of AM, extrudes concentrated suspension inks through a printing nozzle to form desired shapes.^{9,22–26} While DIW and other technologies address demoulding issues, they introduce other challenges, such as delamination between printed layers and entrapped air bubbles. These defects can be mitigated through pre-printing preparation such as centrifugation or sonication to remove trapped bubbles, and through optimising processing parameters including print nozzle moving speed, extrusion speed, nozzle size and layer height to prevent delamination between layers. Fundamentally, the success of all these optimisations depends on achieving suitable rheological properties and good ink stability. These inks should have shear thinning behaviour to make them flow during extraction and a large enough storage modulus (G'), yield stress (σ_v) and flow stress (σ_f) to prevent the collapse and distortion of printed structures. 21,22,24,26-30 Additionally, these inks should be stable and without large ceramic particle aggregates, to prevent clogging of the printing nozzle. Organic additives are commonly utilised during formulation to adjust the rheological properties of DIW inks. Depending on their effect on rheology, additives can be divided into two categories: those that thicken the ink,6,31-35 and those that thin it.7,9,36 Currently, most of the work in the literature selects one kind of polymer additive and demonstrates its effect,^{7,9,33,34} rather than performing a systematic exploration of the effects of a range of additives on ink rheology. One key parameter affecting additive properties is the ionisation of the additive. Water soluble polymers can be nonionic, cationic, anionic and zwitterionic. In addition, they can have a permanent charge or be pH responsive. These parameters influence the interactions between polymers and ceramic particles, thus the suspension stability and rheology.^{22,36,37} Consequently, there is a pressing need for conducting a systematic exploration of the effects of polymer additives with different charges on the rheology of DIW ceramic inks to establish clearer guidelines for selecting additives to optimise ink rheology.

Recent studies have explored the impact of various additives on the rheology of ceramic slurries and suspensions. Yaghtin et al.³⁸ investigated the effects of polyethyleneimine (PEI), 2phosphonobutane-1,2,4-tricarboxylic acid, and alpha-terpineol on the rheology of highly concentrated aqueous yttria-stabilized zirconia slurries at different pHs. Similarly, Lakhdar and Goodridge et al.³⁶ examined the influence of a range of commercial polymer dispersants on the stability and rheology of colloidal boron carbide suspensions. The scope of this research encompassed a diverse array of additives, including cationic branched polyethyleneimine of varying molecular weights, non-ionic polyoxyalkyleneamine derivatives, acrylic copolymers, anionic poly(acrylic acid ammonium salt), and poly(methacrylic acid sodium salt). Both research groups primarily focused on how these additives affected suspension rheology. However, they did not control additive molecular weight variations, and the effect of polymers with differing degrees of ionisation on rheology was not examined. This limitation arose because the polymer additives were procured from commercial manufacturers, rather than being custom produced to meet specific research requirements. Moreover, most research in this field has been directed towards additives that reduce viscosity and flow stress, thereby enabling higher maximum ceramic loading.^{7,9,36,39,40} However, for additives that increase ink thickness, other viscosifiers or binders are typically added alongside dispersants. This practice complicates ink composition, leading to high cumulative polymer additive loads.34,41,42 In some instances, this necessitates further curing processes, posing additional challenges for 3D printer setup and extending printing times. 6,43-45

IOPs typically have surfaces containing hydroxyl groups which serve as anchoring points for polymers containing carboxyl, amine, hydroxyl, and other functional groups. 7,9,46-48 Reported (co)polymers containing these groups have been used as additives to adjust the rheology of IOP suspensions.^{7,9,49,50} However these studies have the same limitations as mentioned above, such as focusing on polymer additives which can thin IOP inks, and

DOI: 10.1039/D5LP00232 neglecting the influence of degree of ionisation and molecular weight on rheology. It is therefore necessary to conduct a systematic study on how polymer additives with different charge, degree of ionisation, and molecular weight affect the rheology of IOP suspensions, and subsequently investigate their different performance for DIW.

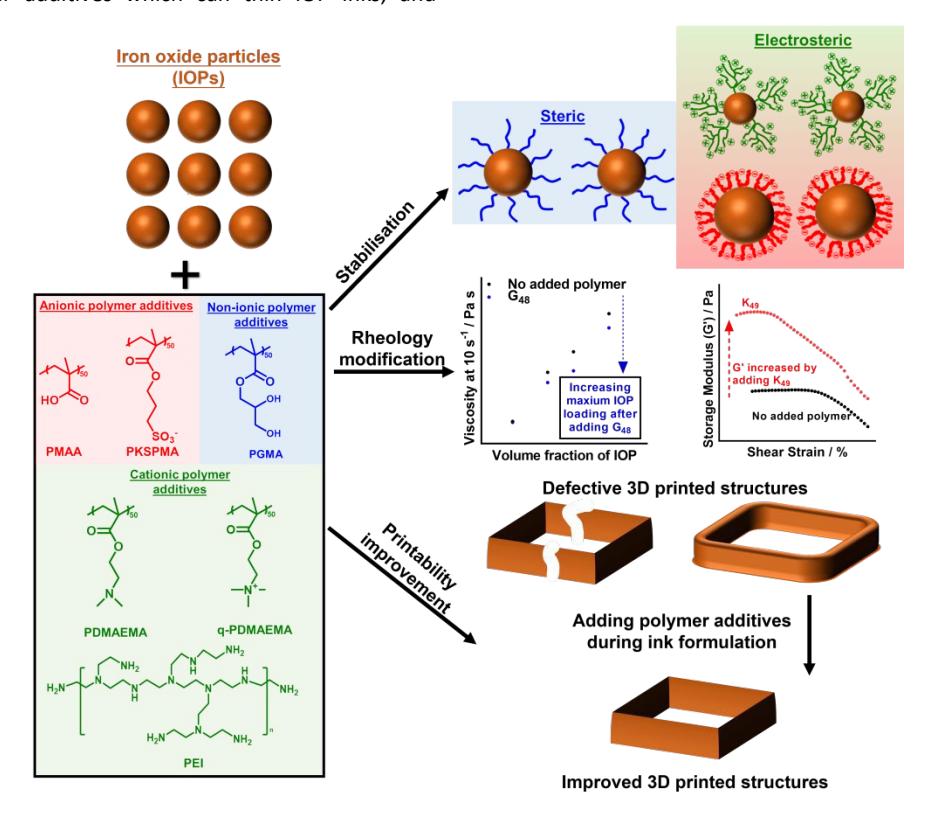


Figure 1. Polymer additives synthesised via RAFT polymerisation were utilised for stabilising, rheology modification and printability improvement of aqueous IOP suspensions. Without polymer additives, the printed structures exhibited significant defects, attributed to a low storage modulus and insufficient IOP loading capacity. Adding poly(glycerol monomethacrylate) (G₄₈) notably enhanced the maximum IOP loading capacity, mitigating crack formation. Similarly, the addition of poly(potassium 3-sulfopropyl methacrylate) (K_{40}) significantly improved the storage modulus for low IOP loading (50% w/w) inks, effectively preventing structural collapse.

Herein, a range of well-defined polymer additives with different functionalities and molecular weights were synthesised via reversible addition-fragmentation chain-transfer (RAFT) solution polymerisation and investigated as polymer additives for the formulation of aqueous IOP inks (Figure 1). The stability of IOP dispersions containing these different polymer additives was methodically evaluated, employing zeta potential, dynamic light scattering (DLS), disc centrifuge photosedimentometry (DCP) and sedimentation measurements. Subsequent investigations focused on the impact of these polymer additives on the rheology of IOP suspensions, utilising oscillatory and steady-state analysis. Finally, the enhancement of ink printability through the addition of these polymer additives was demonstrated by 3D printing IOP inks into thin-walled squares and quantitatively assessed using several printability criteria.51-53

Experimental

Materials. Potassium 3-sulfopropyl methacrylate (KSPMA, 98%), methacrylic acid (MAA), 2-(dimethylamino) ethyl methacrylate (DMAEMA, 98%), quatenised 2-(dimethylamino) methacrylate solution (q-DMAEMA,75% in H₂O), and 4,4'azobis(4-cyanovaleric acid) (ACVA) were purchased from Sigma-Aldrich (UK). Glycerol monomethacrylate (GMA) was generously donated from GEO Specialty Chemicals (UK). 4-cyano-4-(((dodecylthio)carbonothioyl)thio)pentanoic acid (CDTPA) and 4-((((2-carboxyethyl)thio)carbonothioyl)thio)-4-cyanopentanoic acid (CCC) were purchased from Boron Molecular (Australia). Ethanol (95%) was obtained from Fisher Scientific (UK). Iron (III) oxide nanoparticle powder (20-40 nm average particle size) was purchased from Alfa Aesar (UK). Deionised (DI) water with a resistivity of 18.2 M Ω cm was used in all experiments. All reagents were used as received unless otherwise specified.

Synthesis of polymer additives. Polymer additives were synthesised via RAFT solution polymerisation, as described in detail in the Supporting Information (Figure S1-S5). A typical example protocol for the synthesis of PKSPMA48 is as follows. KSPMA (2.0 g, 8.12 mmol), CCC (0.05 g, 0.16 mmol) and ACVA (0.009 g, 0.033 mmol) were dissolved in DI water (8 g) within a 24 mL glass vial. This vial was subsequently sealed and purged with N₂ for 30 minutes. The vial was then immersed in a preheated oil bath at 70 °C for 1.5 hours. Subsequently, the vial was taken out from the oil bath and immersed in an ice bath to stop the polymerisation.

Table 1. Summary of polymer additives.

Acronym	[monomer] : [CTA] ^a	Monomer conversion ^b	Polymer composition ^b	M _n / g mol⁻¹	M _w /M _n
K ₄₉	50	97%	PKSPMA ₄₉	9900 ^c	1.09 ^c
K ₂₈₄	300	94%	PKSPMA ₂₈₄	36380 ^c	1.21 ^c
MA ₄₈	55	87%	PMAA ₄₈	4800 ^d	1.17 ^d
MA ₂₅₀	330	76%	PMAA ₂₅₀	22100 ^d	1.11 ^d
q-D ₄₈	50	95%	q-PDMAEMA ₄₈	10000 ^e	
q-D ₂₈₈	300	96%	q-PDMAEMA ₂₈₈	59600 ^e	
D ₅₀	55	92%	PDMAEMA ₅₀	7900 ^e	
D ₂₈₈	300	96%	PDMAEMA ₂₈₈	45200 ^e	
G ₄₈	50	95%	PGMA ₄₈	7700 ^f	1.30 ^f
G ₂₅₇	330	78%	PGMA ₂₅₇	41100 ^f	1.23 ^f
PEI				60000 ^g	12.5 ^g

- a. The ratio between the concentration of monomer and chain-transfer agent (CTA) during the RAFT polymerisation.
- b. Determined by ¹H NMR analysis.
- c. Measured by aqueous GPC using polyethylene oxide / glycol (PEO/PEG) standards.
- d. Measured by THF GPC using polystyrene standards (PS) standards, PMAA samples were methylated using trimethylsilyl diazomethane to afford poly(methyl methacrylate) before measurement.
- e. Calculated using equation $M_{n,NMR}$ = (repeat unit molar mass × degree of polymerisation determined by NMR analysis) + CTA molar mass. Further details are given in the Supporting Information.
- f. Measured by DMF GPC using poly(methyl methacrylate) (PMMA) narrow standards.
- g. Provided by the manufacturer.

The obtained polymer solution was purified using dialysis (MWCO = 1000 g mol^{-1}) against DI water for 2 days, and then freeze-dried to dryness. The final degree of polymerisation was determined by ^1H NMR using deuterium oxide (D₂O) as solvent (Figure S6) and the molar mass distribution was measured using gel permeation chromatography (GPC) (Figure S11).

Dynamic light scattering (DLS) and aqueous electrophoresis. DLS and aqueous electrophoresis studies were performed using a Malvern Zetasizer Ultra instrument to measure both intensity-average hydrodynamic diameter ($D_{\rm intensity}$) and Zeta potential. The instrument was equipped with a He–Ne solid-state laser operating at 633 nm, detecting back-scattered light at a scattering angle of 173°. All samples were diluted to 0.1% w/w in presence of 1 mM KCl and sonicated in an ultrasonic bath for 1 h before measurements were taken. Data were averaged over three consecutive runs at 25 °C. Plastic cells (Malvern DTS0012) were used for measuring $D_{\rm intensity}$ and capillary cells (Malvern DTS1070) were used for measuring Zeta potential.

Disc centrifuge photosedimentometry (DCP). DCP analyses were conducted using a Centrifugal Photo Sedimentation (CPS) Disc Centrifuge Model 24000 to measure weight-average diameter ($D_{\rm weight}$). A density gradient that ranged from 24 to 8% w/w sucrose solution in DI water was constructed and allowed to stabilise for approximately 30 minutes. A 483 nm diameter poly(vinyl chloride) calibration standard was injected prior to the analysis of each sample. All samples were diluted to 0.1% w/w in presence of 1 mM KCl and sonicated in an ultrasonic bath for 1 h before measurements were taken. The run time was approximately 50 seconds with the centrifuge rate set at 11000 rpm.

Sedimentation experiments of IOP dispersions. Sedimentation experiments were performed to determine the sedimentation behaviour and stability of IOP dispersions with different polymer additives (1% w/w of the mass of IOPs) using the following protocol. 0.01 g of polymer additive was dissolved in 34 g DI water, then 1 g IOPs were added to form 2.86% w/w IOP dispersions. The dispersion pH was adjusted to the required value using 0.025 and 0.25 M HCl and KOH solutions. The dispersion was sonicated for 1 h, vortex mixed for 1 min and transferred to a volumetric cylinder which was then sealed using parafilm to prevent evaporation. The sample was then left undisturbed for 120 h. After 120 h, the volume of sedimented IOPs was recorded as the sedimentation volume. After sedimentation, 2 mL of the supernatant from selected samples was collected for UV-vis spectrophotometry analysis, as detailed in the Supporting Information.

Preparation of iron oxide suspensions. The preparation of a suspension with 50% w/w IOP loading and 0.5% w/w PDMAEMA $_{50}$ loading based on IOP concentration at pH 10 is as follows. 2 g of IOPs were transferred into a 10 mL jar. 0.01 g PDMAEMA $_{50}$ was dissolved in 2 g DI water, and the pH adjusted to 10 by adding 0.25 and 0.025 M KOH solution. This solution was then injected into the jar containing the IOPs. The jar was mixed using a speed mixer (Synergy Devices Ltd, Bucks, UK) at 480 rpm for 1 min, 1500 rpm for 1 min, 1200 rpm for 2 min, 1800 rpm for 2 min, 2000 rpm for 1 min and 400 rpm for 1 min to form a homogenous IOP suspension. Other reported IOP suspensions were prepared through the same procedure by changing the pH, type & loading of polymer additive, and the loading of IOPs.

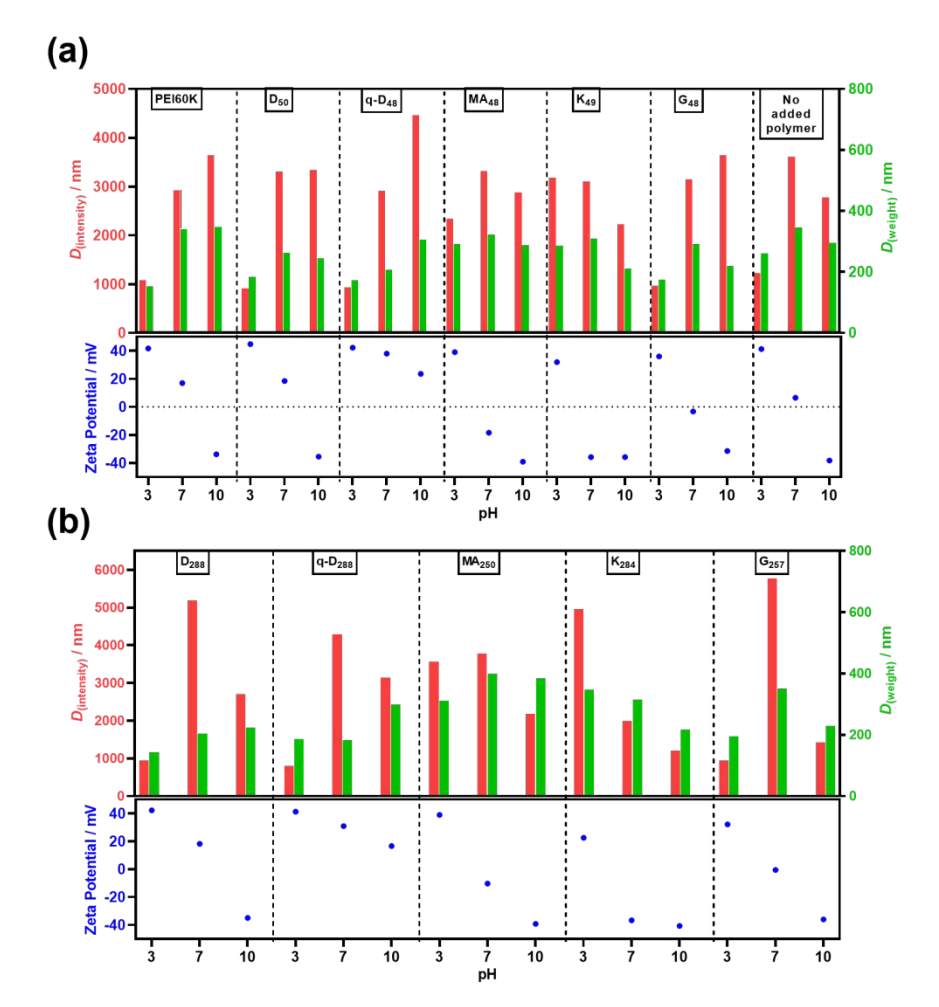


Figure 2. Zeta potential (blue dots), intensity-average diameter $D_{\text{intensity}}$ (red columns) and weight-average diameter D_{weight} (green columns) of IOP dispersions with different added polymers at pH = 3, 7 and 10. The IOP concentration was 0.1% w/w based on the mass of the dispersion and the added polymer concentration was 1% w/w based on the mass of the IOPs.

Rheology of iron oxide suspensions. Rheological measurements were performed using a HAAKE MARS iQ Rheometer, equipped with a flat 35 mm diameter titanium plate and a solvent trap to minimise solvent evaporation. In dynamic oscillation testing, the oscillation frequency was set to 1.592 Hz, and the strain was changed from 0.035 % or 0.1 % to 300 %. During steady-state viscosity measurements, the shear rate was changed from 0.1 s⁻¹ to 100 s⁻¹. The temperature was set to 25 °C for all rheology

Direct ink writing. 11-layer thin-walled square structures were printed onto aluminium substrates by a robot printer (I&J7300R-LF Robots, I&J Fisnar Inc. Wayne, NJ, USA). Inks were loaded into 5 mL dispensing syringes (FIS8001002, FISNAR) with dispensing pistons for syringe barrels (FIS8001007, FISNAR). Loaded syringes were centrifuged at 800 rpm for 2 min before printing. Straight, flexible dispensing tips (FIS5601087, FISNAR) with 0.84 mm diameter and 12.7 mm length were used as the print nozzle head. The nozzle head speed was fixed at 8 mm s⁻¹. After printing, green bodies were dried in air for at least 12 hours before being removed from the substrate.

Results and Discussion

Polymer additives studied. A series of well-defined homopolymers with different functionalities and molecular weights were prepared by RAFT solution polymerisation, as described in the Supporting Information. Specifically, poly(methacrylic acid) (PMAA or MA_x), poly(potassium 3methacrylate) (PKSPMA or K_x), (dimethylamino) ethyl methacrylate) (PDMAEMA or Dx), quatenised poly(2-(dimethylamino) ethyl methacrylate) (q-PDMAEMA or q-D_x), and poly(glycerol monomethacrylate) (PGMA or G_x) were prepared and characterised by 1H NMR and GPC (Figures S1-S13), as summarised in Table 1. As expected, these polymers had degrees of polymerisation (DPs) close to the targeted value and relatively narrow molecular weight distributions. These polymers and a commercial branched PEI were investigated as additives for the formulation of aqueous IOP inks. Initially studies were conducted on low concentration IOP dispersions before investigating how these observations translated to high concentration dispersions suitable for DIW.

Zeta potential, DLS and DCP studies. The stability and size distribution of low concentration (0.1 % w/w) IOP dispersions, both with (1 % w/w, based on IOP concentration) and without polymer additives, were studied at pH 3, 7 and 10. The Zeta potential values, which are indicative of surface charge and colloidal stability,54-56 along with particle aggregation measurements obtained by DLS and DCP are given in Figure 2.

IOPs typically have surfaces containing hydroxyl groups (-OH)4,47,48,57 which become protonated (-OH2+) at pH 3 and deprotonated (-O-) at pH 10. This produces a pronounced pHdependent variation in the Zeta potential of the pristine IOPs. At

pH 3, the pristine IOPs demonstrated a highly positive Zeta potential of 41 mV as a result of hydroxyl group protonation. The Zeta potential exhibited a modestly positive value of 7 mV as the pH increased to pH 7 because of the reduced degree of protonation. When the pH was increased from 7 to 10, the hydroxyl groups became deprotonated, which yielded a negative Zeta potential value (-38 mV). The primary particle size of these pristine IOPs was 20-40 nm, as provided by the supplier and confirmed by electron microscopy (Figure S14). The primary IOPs aggregated to form aggregates with various sizes at different pH values. As illustrated in Figure 2a, D_{intensity} (measured by DLS) of IOPs in the absence of polymer indicated the presence of relatively small aggregates at pH 3 (1230 nm). This can be attributed to the relatively high Zeta potential (41 mV) providing strong electrostatic repulsion. D_{intensity} significantly increased at pH 7 to 3600 nm due to increased aggregation as a result of the low Zeta potential value (7 mV) providing weak electrostatic repulsion. As the pH increased from 7 to 10, the large negative Zeta potential (-38 mV) resulted in a decrease in aggregate size ($D_{intensity} = 2800$ nm). D_{weight} (measured by DCP, Figure S15) showed a similar trend to D_{intensity}, increasing from 140 nm at pH 3 to 250 nm at pH 7, and decreasing to 200 nm at pH 10 (Figure 2a). It is noteworthy that, in all cases, D_{intensity} was much higher than D_{weight}. This difference is due to several reasons. First, DCP measures weight-average aggregate size, whereas DLS reports intensity-average, aggregate size. Thus, dispersions of IOP aggregates with large size polydispersity are substantially oversized by DLS, especially with the backscattering detector used herein.58 Second, DLS measures the dispersion without performing any separation, and light scattering is dominated by the presence of any large aggregates. In contrast, DCP separates out the particle size distribution centrifugally during measurement and is therefore less biased towards the presence of the larger species present. Nevertheless, both of these techniques indicated the presence of IOP aggregates, rather than a uniform dispersion of primary particles (Figure 2, and Figure S15) and confirmed the effect of pH on the relative size of these aggregates.

For PEI-containing IOPs dispersions, the Zeta potential was 42, 17 and -34 mV at pH 3, 7 and 10, respectively. Meanwhile, the PEIcontaining IOP dispersions demonstrated decreased amounts of particle aggregation at pH 3 and 7 in comparison to pristine IOPs, and increased particle aggregation at pH 10 (Figure 2a). PEI is protonated at pH 3 and 7 and thus this cationic polymer provides electrosteric repulsion between particles, aggregation. At pH 10, the residual positive charge of PEI partially shields the negative charge of the IOPs, leading to a decrease in electrostatic repulsion and resulting in more aggregation. The Zeta potential and aggregation behaviour of the D₅₀-containing IOP dispersions were similar to PEI-containing dispersions (Figure 2a). This is because PDMAEMA₅₀ is also a pH responsive cationic polymer with a pK_a of approximately 7.59 q-D₄₈-containing IOP dispersions exhibited positive Zeta potentials at pH 3, 7 and 10 (42, 38 and 24 mV, respectively) due to the permanent cationic charge of q-D₄₈ imparting this behaviour when adsorbed to the surface of IOPs. In this case, Dweight increased from 172 nm at pH 3 to 207 nm at pH 7 and 305 nm at pH 10. Similarly, D_{intensity} increased with increasing pH from 940 nm at pH 3 to 4462 nm at pH 10 (Figure 2a). The reason for the increase in aggregate size for $q\text{-}D_{48}\text{-}\text{containing IOP}$ dispersions is not fully apparent. However, it can be hypothesised to be caused by the underlying IOP charge resulting in increased aggregation of the IOPs before the q-D48 was able to provide sufficient stabilisation.

For MA₄₈-containing IOP dispersions, the Zeta potential was observed to be 39 mV at pH 3, which was slightly lower than the

Zeta potential of pristine IOP dispersions. This is because the carboxylic acid groups on PMAA may have shielded the -OH+ groups on the surface of the IOPs. At pH 7 and 10, the Zeta potential of MA₄₈-containing IOP dispersions was -18 mV and -39 mV. This reversal in Zeta potential suggested the carboxylic acid groups on MA₄₈ were deprotonated and adsorbed onto the IOPs, causing the particles to become anionic. For K₄₉-containing IOP dispersions, the Zeta potential was 32, -36 and -36 mV at pH 3, 7 and 10, respectively. The Zeta potential was lower at pH 3 and 7 than the pristine IOP dispersions because of the negatively charged PKSPMA adsorbed to the surface of the IOPs. The values of D_{weight} and $D_{intensity}$ suggested an increase in stability of K_{49} containing IOPs with increasing pH due to a decrease in measured aggregate size. However, during these experiments, K₄₉ containing samples were unstable at all pHs, aggregating and sedimenting relatively rapidly. This was confirmed in subsequent sedimentation experiments, discussed below.

PGMA was selected as a non-ionic polymer to investigate whether steric stabilisation alone (rather than electrosteric stabilisation) would provide benefits to IOP ink formulation. The Zeta potential of the G₄₈-containing IOP dispersions did not change significantly compared to the pristine IOP dispersion due to the non-ionic nature of PGMA. Notably, D_{weight} and $D_{intensity}$ decreased significantly (Figure 2a) and was attributed to the stabilisation imparted by adsorbed G₄₈. addition to the polymers described above, cationic, anionic and non-ionic polymers with larger molar masses were prepared to assess the effect of molecular weight on the rheological properties and printability of polymer containing IOP dispersions. The Zeta potential, D_{weight} and $D_{intensity}$ of IOP dispersions with 1% w/w added polymer, based on IOP concentration, with larger M_n are shown in Figure 2b. Interestingly, increased molecular weight did not significantly affect the measured Zeta potential, D_{weight} and $D_{intensity}$ values when comparing between IOP dispersions containing the same type of polymer with smaller M_n (Figure 2a). However, it was expected that the molecular weight would have an effect on the rheological properties of high concentration IOP suspensions, discussed below.

In summary, the Zeta potential and aggregation behaviour of IOP dispersions were markedly influenced by the pH and the presence of differently charged polymer additives. Pristine IOPs showed maximum stability at pH 3 due to strong electrostatic repulsion. Cationic polymers (PEI and PDMAEMA) enhanced stability at lower pH through electrosteric repulsion. However, at alkaline pH, these cationic polymers were less effective at stabilizing IOPs against aggregation. Carboxylic acid functional anionic polymers (PMAA) provided effective stabilisation of IOPs at neutral and alkaline pH whereas sulfonate functional PKSPMA seemed to act as a poor stabiliser. The non-ionic polymer PGMA demonstrated a stabilising effect at all pH values but did not significantly change the Zeta potential when compared to pristine IOPs.

Sedimentation experiments. Sedimentation experiments were conducted to obtain insights into the effects of different polymers on the stability of moderately concentrated IOP dispersions (2.86% w/w). The effect of polymer additive on the settling behaviour of IOPs was demonstrated by the volume of sedimented IOPs, knows as the sedimentation volume (Figure 3). As illustrated in Figure 3d, a small sedimentation volume indicated good stability and less aggregation of IOPs. On the other hand, a large sedimentation volume indicated low stability and large amounts of IOP aggregation.³⁶

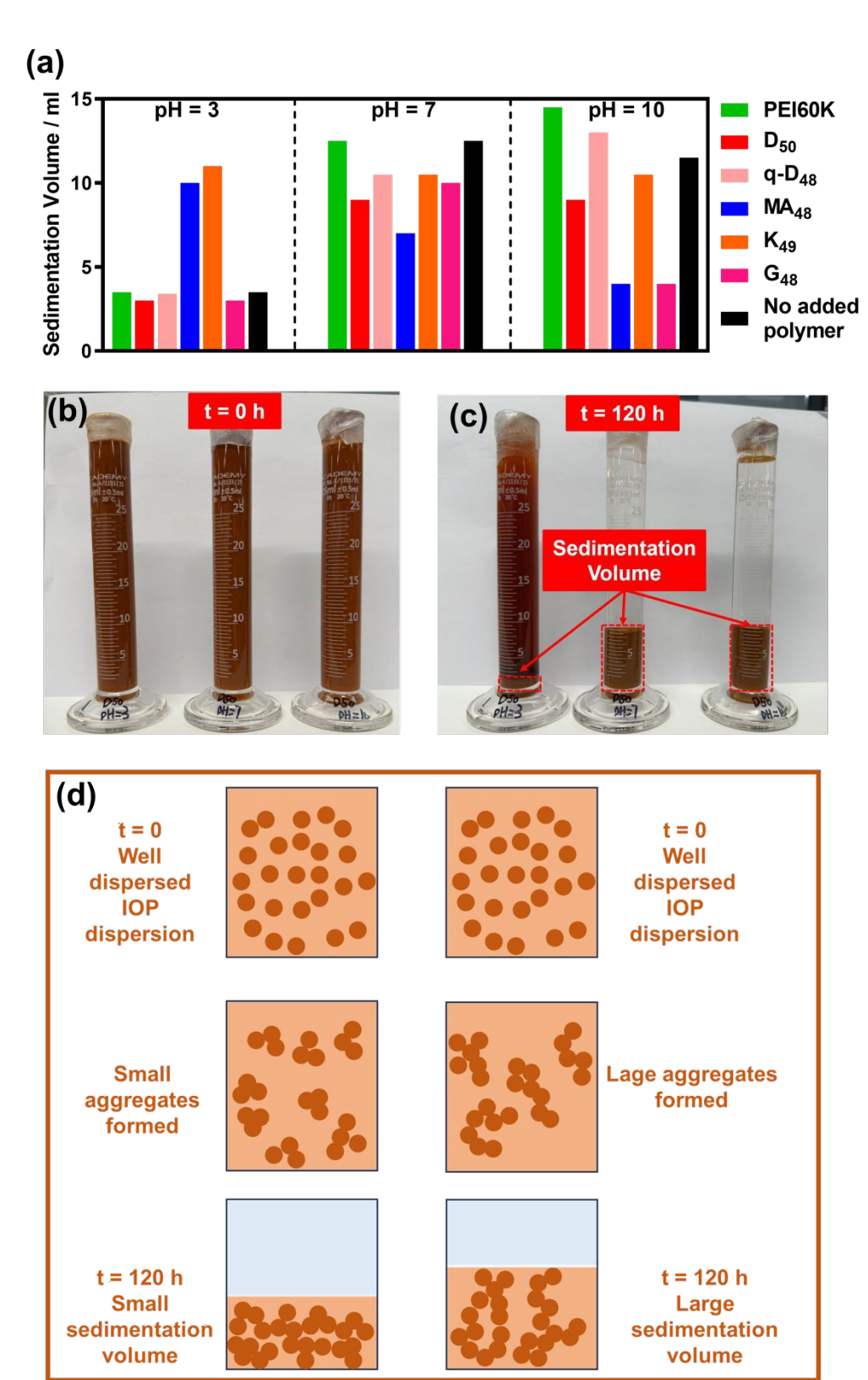


Figure 3. Sedimentation tests for 2.85% w/w IOP dispersions with and without 1% w/w added polymer (based on IOP concentration), at pH 3, 7, and 10. Dispersions were sonicated for 1 h, vortex mixed for 1 min, and then left to stand undisturbed for 120 h, after which the sedimentation volume was measured, as summarised in (a). Photographs of 2.85% w/w IOP dispersions with 1% w/w D₅₀ at pH 3, 7 and 10, at (b) t = 0 and (c) t = 120 h. (d) Schematic showing the formation of small (left) and large (right) sedimentation volumes.

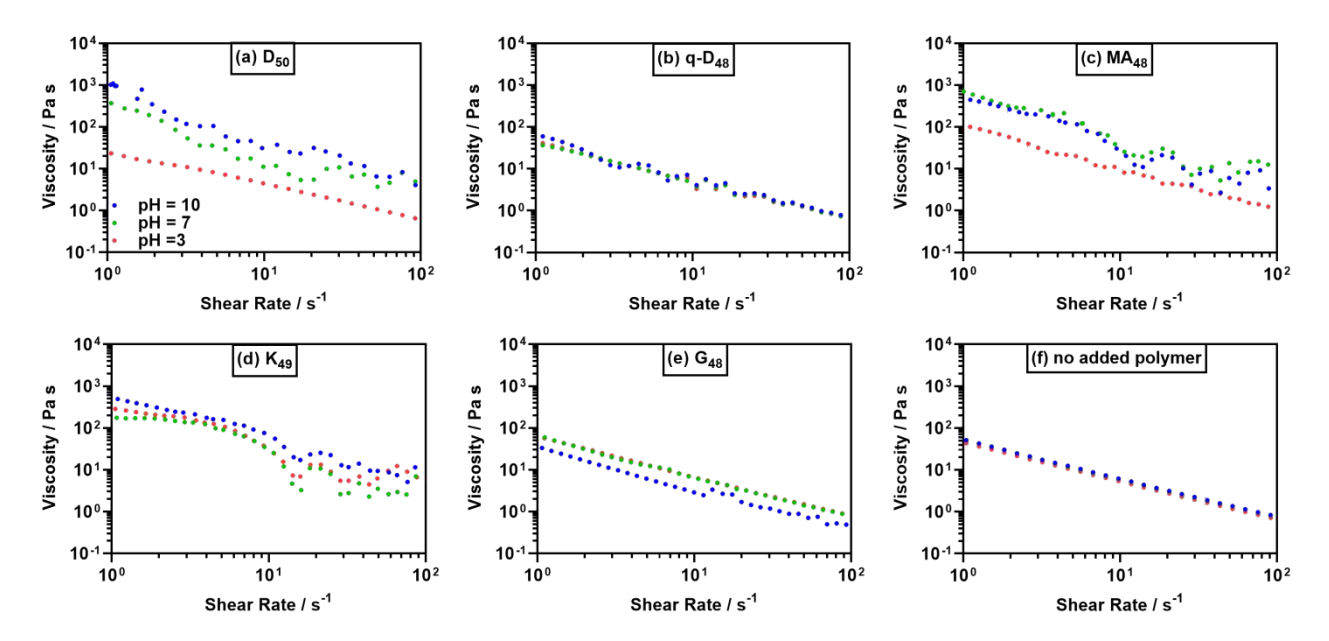


Figure 4. Viscosity vs shear rate for 50% w/w IOP suspensions with 0.5% w/w (a) D_{50} , (b) q- D_{48} , (c) MA_{48} , (d) K_{49} , (e) G_{48} , and (f) without added polymer at pH = 3 (red dots), pH = 7 (green dots) and pH = 10 (blue dots). The 0.5% w/w polymer additive concentration is based on IOP concentration.

At pH 3, IOP dispersions with G₄₈, D₅₀, q-D₄₈, PEI and no polymer resulted in a low sedimentation volume (< 5 mL, Figure 3). The low sedimentation volume resulted from the relatively high colloidal stability and small degree of IOP aggregation, as indicated by DLS and DCP studies (Figure 2). IOP dispersions containing MA₄₈ and K₄₈ formed sediments with large sedimentation volumes of approximately 11 mL due to relatively low stability and formation of large IOP aggregates. The observed sedimentation behaviour of the MA₄₈-containing IOP dispersion at pH 3 presented an intriguing anomaly in that both D_{weight} and $D_{intensity}$ measurements were unexpectedly small. This discrepancy was because of a complex sedimentation dynamic that was not fully captured by the DLS and DCP size measurements. At pH 3, aggregation of IOPs rapidly occurred (within approximately 10 s) in the MA₄₈containing IOP dispersion forming sizable clusters. These agglomerates exceeded the set test range of DCP (50 ~ 1000 nm) and settled too swiftly to be accurately sized by DLS, resulting in the recorded D_{weight} and $D_{intensity}$ values being much lower than anticipated.

At pH 7, the IOP dispersions containing D_{50} , q- D_{48} , K_{48} , PEI and G_{48} , as well as the pristine IOP dispersion, exhibited sedimentation volumes of 10 mL or more (Figure 3a), signifying reduced colloidal stability and notable particle aggregation. This trend was corroborated by the increased value of D_{weight} and $D_{\text{intensity}}$. In contrast, the MA_{48} -containing dispersion demonstrated moderately better stability, evidenced by a sedimentation volume of only 7 mL.

At pH 10, the MA₄₈ and G₄₈-containing IOP dispersions had a reduced sedimentation volume of 4 mL (Figure 3a), indicative of improved colloidal stability and minimal particle aggregation. The enhancement in stability for these two dispersions was primarily ascribed to the amplified electrostatic and steric repulsion. Conversely, the pristine IOP dispersion and the IOP dispersions containing the other polymers studied showed considerable sedimentation volumes (\geq 9 mL), pointing to a lower stability as corroborated by large D_{weight} and $D_{\text{intensity}}$ values in Figure 2. An exception was observed for the K₄₈-containing IOP dispersion,

which, despite its large sedimentation volume, recorded unexpectedly low $D_{\rm weight}$ and $D_{\rm intensity}$ values at pH 10 compared to those at pH 3 and 7. The reason for this anomaly is same as that previously discussed for the MA₄₈-containing IOP dispersion at pH 3, where large aggregates were not effectively recorded by DLS and DCP.

In addition to the considerations above, the swelling of the added polymer may also have affected the final sedimentation volume. In theory, polymer swelling can reduce interactions between colloidal particles after sedimentation, resulting in open sediment structures with larger volumes. However, in this research, the sedimentation volume was not primarily controlled by swelling behaviour. For instance, as the pH increased, MA₄₈ was expected to swell, which would typically lead to a gradual increase in sedimentation volume from pH 3 to 7 and 10. Contrary to this expectation, the sedimentation volume of the MA₄₈-containing IOP dispersion decreased with increasing pH (Figure 3a), indicating that the sedimentation volume was mainly dominated by aggregate size, as discussed above, rather than by polymer swelling. This conclusion also extends to the pH-responsive D₅₀ and PEI-containing IOP dispersions.

Overall, the findings from the sedimentation experiments were found to be consistent with the Zeta potential and size distribution measurements described above. The two exceptions were MA_{48} and K_{48} -containing dispersions at pH 3 and 10, respectively, and were due to the rapid aggregation and the formation of sizeable clusters not detected by the particle sizing methodology used herein. This highlights the importance of comprehensive sedimentation experiments in assessing the true effects of polymer additives and pH on IOP stability, offering insights beyond those provided by Zeta potential and size distribution measurements alone. 36,38 The following rheology investigations provide even further insights into suspension behaviour, especially when considering highly concentrated suspensions.

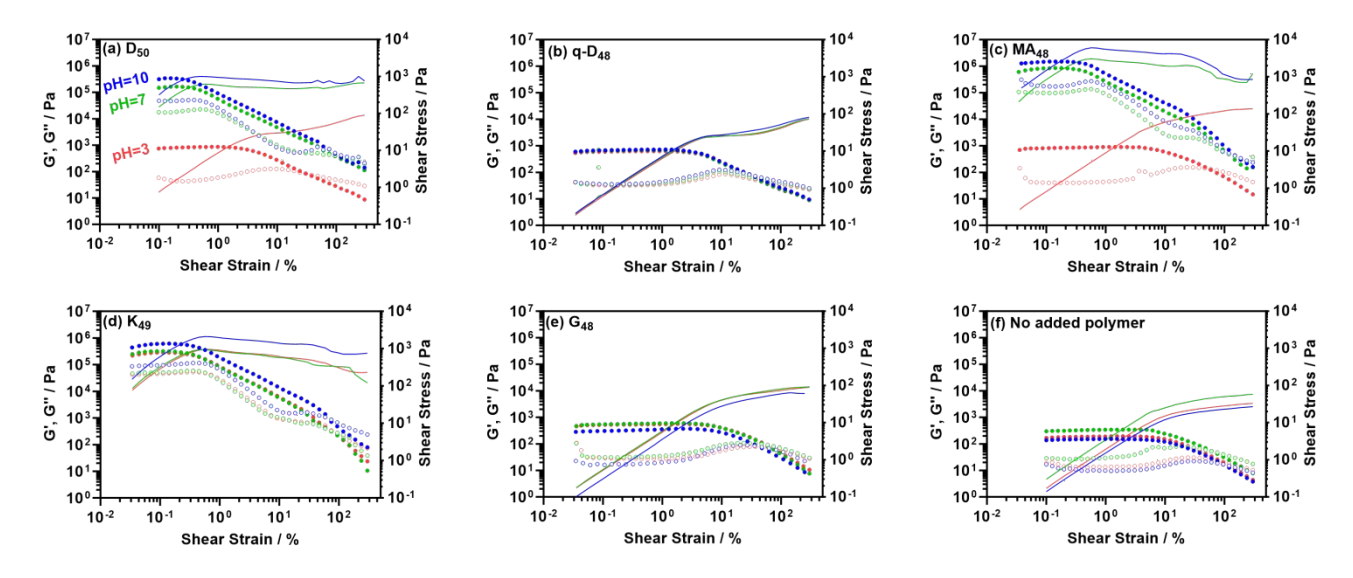


Figure 5. Storage modulus (G', solid dots), loss modulus (G", hollow dots) and shear stress (solid line) as a function of shear strain for 50% w/w IOP suspensions with 0.5% w/w (a) D_{50} , (b) $q-D_{48}$, (c) MA_{48} , (d) K_{49} , (e) G_{48} , and (f) without added polymer at P_{50} pH = 3 (red), P_{50} (green) and pH = 10 (blue). The 0.5% w/w polymer additive concentration is based on IOP concentration.

Rheology of different polymer-containing IOP suspensions. Initially, different polymer additives (Table 1) were each mixed with 50% w/w IOP aqueous suspensions at 0.5% w/w polymer based on IOP concentration using a high-speed mixer. The pH was varied (pH 3, 7 and 10) and the resulting viscosity compared to pristine IOP dispersions.

The pristine IOP suspensions demonstrated shear thinning behaviour. Their viscosity decreased from ~40 Pa s at 1 s⁻¹ to ~1 Pa s at 100 s⁻¹ (Figure 4f). There were negligible differences in the measured viscosity of the pristine IOP suspensions at the three different pH values studied. This is perhaps surprising based on the particle size, Zeta potential and sedimentation investigations above for less concentrated IOP dispersions. In addition, previous reports typically assume the stability of low-concentration ceramic dispersions to be related to the viscosity of highconcentration ceramic suspensions, where poor dispersion stability leads to high viscosity, and good stability results in low viscosity.re, the pristine IOP dispersions demonstrated different stability and aggregate sizes at pH 3, 7, 10, but the viscosity of the pristine IOP suspensions was not affected by the pH. One plausible explanation is that the hydroxyl groups on pristine IOPs are nonionic under the conditions studied, and thus the thickness of electrical double-layer was relatively thin. Under these circumstances, the pristine IOP suspensions could be assumed to be a hard-sphere system, where interparticle interactions are not experienced until they closely approach each other, meaning that the viscosity is dominated primarily by the solid loading, primary particle/aggregate size and shape.55

The addition of D₅₀ resulted in pH-sensitive viscosity changes in the IOP suspensions. At pH 3, protonated D₅₀ provided electrosteric repulsion between IOPs, significant decreasing the viscosity (Figure 4a) to 25 Pa s at 1 s⁻¹, approximately half the viscosity of the pristine IOP suspension (Figure 4f). At pH 7, close to the pK_a of PDMAEMA,⁵⁹ D₅₀ chains collapsed due to deprotonation, increasing their hydrophobic character. The hydrophobic association between the D₅₀ polymer chains induced aggregation, which led to a significant increase in viscosity (390 Pa s at 1 s⁻¹).t pH 10, the viscosity increased to 1270 Pa s at 1 s⁻¹ because of further deprotonation of D₅₀ further increasing the amount of aggregation.

The q-D₄₈-containg IOP suspensions had viscosities of 30, 40 and 60 Pa s at 1 s⁻¹, at pH 3, 7 and 10, respectively (Table S1). There was a slight decrease in viscosity at pH 3 and 7 when compared to pristine IOP suspensions due to strong electrosteric repulsion caused by the surface-adsorbed q-D₄₈. The slight increase in viscosity at pH 10 for q-D₄₈-containg IOP suspensions was potentially caused by the decrease in particle stability as discussed above (Figure 2 and 3a). Similarly, the addition of G₄₈ (Figure 4e) slightly decreased the viscosity when compared with pristine IOPs suspensions (Figure 4f). The non-ionic G₄₈ reduced viscosity through steric repulsion. 9,60-62

MA₄₈-containing IOP suspensions displayed a distinct pHdependant viscosity profile (Figure 4c). At pH 3, the viscosity was 110 Pa s at a shear rate of 1 s⁻¹ and this value significantly increased to 710 and 500 Pa s at pH 7 and 10, respectively. The pK_a of PMAA is approximately 5.5, thus MA₄₈ was deprotonated (and anionic) at pH 7 and 10. At pH 3 MA₄₈ was protonated, and the chains were therefore collapsed resulting in a decrease in viscosity.⁶³ Similarly, anionic K₄₈-containing IOP suspensions (Figure 4d) had high viscosities at shear rates of 1 s-1 (300, 200, 530 Pa s at pH 3, 7, 10, respectively), which were 4-to-9 times those of the pristine IOP suspensions. These observations demonstrate that IOP suspensions could be significantly thickened using anionic polymer additives, as expected. To confirm this thickening behaviour was caused by adsorbed polymer, UV-Vis spectrophotometry studies were conducted (Figure S19 and Table S2). For example, nearly all of the added K₄₈ was adsorbed onto the IOPs (see Figure S19), leaving little free K₄₈ in solution.

One interesting observation is that the use of cationic additives tended to reduce the viscosity of IOP suspensions whereas anionic additives caused thickening. This is commonly observed for ionic rheology modifiers and is often attributed to differences in their electrostatic interactions with the surrounding medium, where anionic polymers adopt extended conformations due to intramolecular charge repulsion and enhanced hydration, thereby increasing viscosity, while cationic polymers tend to collapse or aggregate through charge neutralization and bridging interactions, resulting in reduced thickening effects. 64-66

ship between viscosity and shear rate within the specific range of 1 to 100 s⁻¹ was fitted using power law equation $\eta = a \times v^{(b-1)}$ (see Table S1), 67,68 where η is the viscosity, a is the flow consistency index, γ is the shear rate, and b is the flow behaviour index. Low flow consistency index indicates a low resting viscosity of the IOP suspensions, while a low flow behaviour index indicates stronger shear thinning behaviour. Notably, the use a Herschel-Bulkley model²⁴ to fit this shear stress data would have been preferable. However, noise and the limited shear rate range in our dataset made it unfeasible to use this model. The pristine IOP suspensions exhibited significant shear thinning behaviour ($b \le 0.1$) at pH 3, 7 and 10. This significant shear thinning was also observed for the G_{48/257}, PEI, q-D₂₈₈, and MA_{48/250} containing IOP suspensions at pH 3, 7 and 10, as well as K₂₈₄ containing IOP suspensions at pH 3 and 7. In contrast, the $D_{50/288}$ and q- D_{48} containing IOP suspensions demonstrated high flow behaviour index ($b \ge 0.25$) at pH 3, 7, 10, indicating lower shear thinning behaviours.

Figure 5 shows the storage modulus (G'), loss modulus (G"), and shear stress as functions of oscillation strain for IOP suspensions containing various polymer additives in amplitude sweep tests. In all plots shown in Figure 5, three regions are clearly distinguishable. The first region, known as linear viscoelastic region (LVR), is where the storage modulus (G') is larger than the loss modulus (G") and remains constant. In this region, the shear stress shows a linear response and the storge modulus in LVR (G'_{LVR}) is equal to the elastic modulus of a solid-like material. The second region is the yield region, where G' decreases as the shear strain increases due to the irreversible microstructure evolution. The yield point marks the transition from linear viscoelastic behaviour to nonlinear viscoelastic behaviour. However, in this region the elastic behaviour still dominates the viscoelastic performance over the viscous behaviour (G' > G"). The final region is the flow region, which starts from the point where (G' = G''). ^{9,24} In this region the viscous behaviour dominates over the elastic behaviour and the suspension flows. 22,24,67 The relationship between shear strain and shear stress varied across different suspensions. For soft suspensions ($G'_{LVR} < 10^4$ Pa and shear stress < 200 Pa), shear stress continued to increase with shear strain beyond the yield point, which is typical behaviour for shear thinning suspensions. In contrast, more solid-like samples (G'LVR > 10⁴ Pa and shear stress > 200 Pa) reached a maximum stress near the yield point followed by a decrease in stress with increasing strain. This behaviour could be caused by network break during yielding or some issues during measurement such as fracture, slip, and shear banding. 28,30,52,69

For pristine IOP suspensions (Figure 5f), the low G' LVR values of 190, 349, and 150 Pa at pH 3, 7, and 10, respectively, indicated a weak elastic modulus, suggesting that these suspensions are too weak to retain their shape e.g., after printing. Additionally, they had low flow stress values of 30, 50, and 20 Pa at pH 3, 7, and 10. The G'_{LVR} of D₅₀-containing IOP suspensions were 830, 133200 and 340000 Pa, at pH 3, 7 and 10, respectively and the flow stress values were 80, 420 and 710 Pa (Figure 5a and Table S1). At pH 7 and 10, the high value of G'_{LVR} (> 10^5 Pa) and flow stress (> 400 Pa) were attributed to the formation of a bridging network of aggregates through hydrophobic associations. 59,70,71 This network structure enhanced resistance to deformation and prevented collapse. When the pH decreased to 3, D₅₀ became protonated and hydrophilic. Consequently, the hydrophobic associations were no longer present, resulting in very low values of storage modulus and flow stress. The G'_{LVR} of q-D₄₈-containing IOP suspensions was 610, 660 and 710 Pa at pH 3, 7 and 10, respectively (Figure 5b and Table S1). The slight increase of G'LVR compared to pristine IOP suspensions was potentially caused by

the entanglement of q-D₄₈ chains. This entanglement no longer affected the flow of IOPs at high shear strain, which was confirmed by the low flow stress of q-D₄₈-containing IOP suspensions (40-70 Pa) at pH 3, 7 and 10. For MA₄₈-containing IOP suspensions, the values of G'_{LVR} and flow stress were strongly pH dependent (Figure 5c and Table S1). At pH 7 and 10, G'_{LVR} was 672300 and 1233000 Pa, respectively, and the flow stress was 820 and 900 Pa. Similar to the viscosity behaviour described above, the values of G'_{LVR} (820 Pa) and flow stress (100 Pa) were low at pH 3 as a result of PMAA protonation. K₄₉-containing IOP suspensions demonstrated high G'_{LVR} values of 216300, 296900 and 471200 at pH 3, 7 and 10, respectively (Figure 5d and Table S1) due to strong polymer hydration and entanglement. These factors also contributed to high flow stresses of 300, 200 and 530 Pa at pH 3, 7 and 10, respectively. The G'_{LVR} of G_{48} -contianing suspensions were 540, 580 and 310 Pa at pH 3, 7 and 10, respectively (Figure 5e and Table S1). The G'_{LVR} was pH independent due to the non-ionic nature of the G_{48} adsorbed onto the IOPs, providing steric repulsion at all pHs. This steric repulsion also decreased the flow stress at pH 10

A series of homopolymers with higher $M_{\rm n}$ (DPs > 250) were also synthesised (Table 1) and their effect on IOP suspension rheology assessed (Figure S16 and S17, Table S1). With increasing $M_{\rm n}$, the $G'_{\rm LVR}$ and flow stress of IOP suspensions containing PKSPMA and PMAA decreased. Conversely, the $G'_{\rm LVR}$ and flow stress of IOP suspensions containing q-PDMAEMA and PDMAEMA increased with increasing $M_{\rm n}$. However, the $M_{\rm n}$ of PGMA $_{\rm x}$ did not significantly affect the rheology of PGMA-containing IOP suspensions.

The PEI-containing (M_n ~60000 g mol⁻¹) IOP suspensions demonstrated a rise in viscosity (Figure S16g), G'_{LVR} and flow stress (Figure S17g) with increasing pH, as summarised in Table S1. This pH-responsive performance correlated with the multiple pK_a values for PEI, which are approximately 9.0, 8.0 and 6.0 for primary, secondary and tertiary amines.⁷², respectively. At pH 3, all amine groups are fully protonated and the PEI chains become fully extended, providing strong electrosteric repulsion and halving the viscosity (20 Pa s at 1 s⁻¹) compared to the pristine IOP suspension (40 Pa s at 1 s⁻¹). At pH 7, the viscosity increased significantly, to ten-fold higher than the vale at pH 3, and increased further at pH 10. This was due to the formation of hydrophobic associations caused by deprotonation of the amine groups, which has been discussed above for D₅₀-containing IOP suspensions.⁷⁰ The G'_{LVR} and flow stress of PEI-containing IOP suspensions showed the same trend as the viscosity response to changes in pH.

In summary, the addition of polymer additives increased the G'LVR in all cases compared to pristine IOP suspensions. In particular, the formation of hydrated polymer networks, entanglements and hydrophobic association significantly enhanced the G'LVR, flow stress and viscosity of these suspensions. In addition, G₄₈, D₅₀ and q-D₄₈ demonstrated their ability to decrease the flow stress at pH 10, 3 and 7, respectively, due to either steric or electrosteric repulsion. These rheological studies therefore elucidated the effects of various polymers on the potential formulation of 3Dprintable IOP inks. It is also worth noting that the rheological behaviour of bare IOP suspensions and IOP suspensions containing q-D₄₈, K₄₉ and G₄₈ was not significantly affected by aggregate size at different pHs, compared to IOP suspensions containing the other additives. This observation can be attributed to two possible mechanisms. First, in these suspensions, the rheological properties are primarily governed by the ionisation state of the polymer additives and the resulting polymer-polymer and polymer-particle interactions. Since q-D $_{48}$, G $_{48}$, K $_{49}$ and the

hydroxyl groups on bare IOP surfaces exhibit minimal pHdependent ionization changes, 62,73-79 their interactions remain relatively constant across the pH range. Second, the applied shear stress during rheological measurements may cause the breakup of aggregates, leading to a dynamic equilibrium in aggregate size regardless of pH.61 However, we lack direct evidence to confirm this hypothesis. Future studies employing techniques such as rheomicroscopy⁶⁹ and Rheo-SANS⁸⁰ could provide insights into aggregate size and shape evolution during rheology measurements.

Application of polymer additives for 3D printing of the IOPs inks. For pristine IOP suspensions, a relatively low IOP loading (50% w/w, based on mass of the suspension) results in G'LVR and flow stress values that are too low to maintain structures post-printing or resist sagging and collapse. The addition a small amount of polymer additive such as PKSPMA, PMAA, PEI and PDMAEMA at ~0.5% w/w, relative to the mass of IOPs, and adjusting the pH appropriately, can markedly enhance the G'LVR and shear stress, thereby potentially improving shape retainability and increase resistance to sagging or collapse of the printed filament. In addition, G48 was promising for the preparation of high loading inks as it decreases IOP dispersion viscosity at pH 10. The addition of D_{50} , q- D_{48} and PEI also decreased viscosity at pH $3.^{40,72}$

Unexpectedly, upon increasing the IOP loading from 50 to 70% w/w or higher, the viscosity-reducing effect of adding D₅₀ was not

DOI: 10.1039/D5LP002323 observed (Figure S18a). This phenomenon was also noted for q-D₄₈ pH 3 (Figure S18b). In contrast, G₄₈ consistently reduced viscosity across all IOP loadings (Figure S18a), suggesting that the steric repulsion provided is more effective in decreasing suspension viscosity than the cationic electrosteric repulsion of q- D_{48} and D_{50} , particularly at high IOP loadings. Additionally, G_{48} lowered the flow stress of formulations with IOP loadings over 70% w/w (Figure 6f). This is important as inks with ultra-high flow stress (> 1000 Pa) can prevent ink extrusion during DIW. For stable ink extrusion during DIW, the flow stress of the ink should be lower than the maximum shear stress at the wall of the printhead to ensure controllable flow of the ink. Theoretically, the maximum shear stress is determined using $\tau = (\Delta P/2L)r,^{7,9,23}$ where τ is the maximum shear stress, ΔP is the pressure applied at the nozzle, L is the length of the nozzle, and r is the radius of the nozzle. For the printer used in this work, the maximum shear stress at the wall of calculated nozzle to he ~723 Pa the was $(\Delta P = 43750 \text{ Pa}, r = 0.42 \text{ mm}, L = 12.7 \text{ mm})$. Practically, inks with flow stresses slightly above the theoretical value can be printable due to the non-Newtonian nature of inks and dynamic printing conditions. The usable flow stress was therefore limited to approximately 1000 Pa for the printer used in this study. Consequently, without added polymer, the highest feasible IOP loading for 3D printing was 65% w/w and introducing G₄₈ enabled an increase in printable IOP loading to at least 70% w/w.

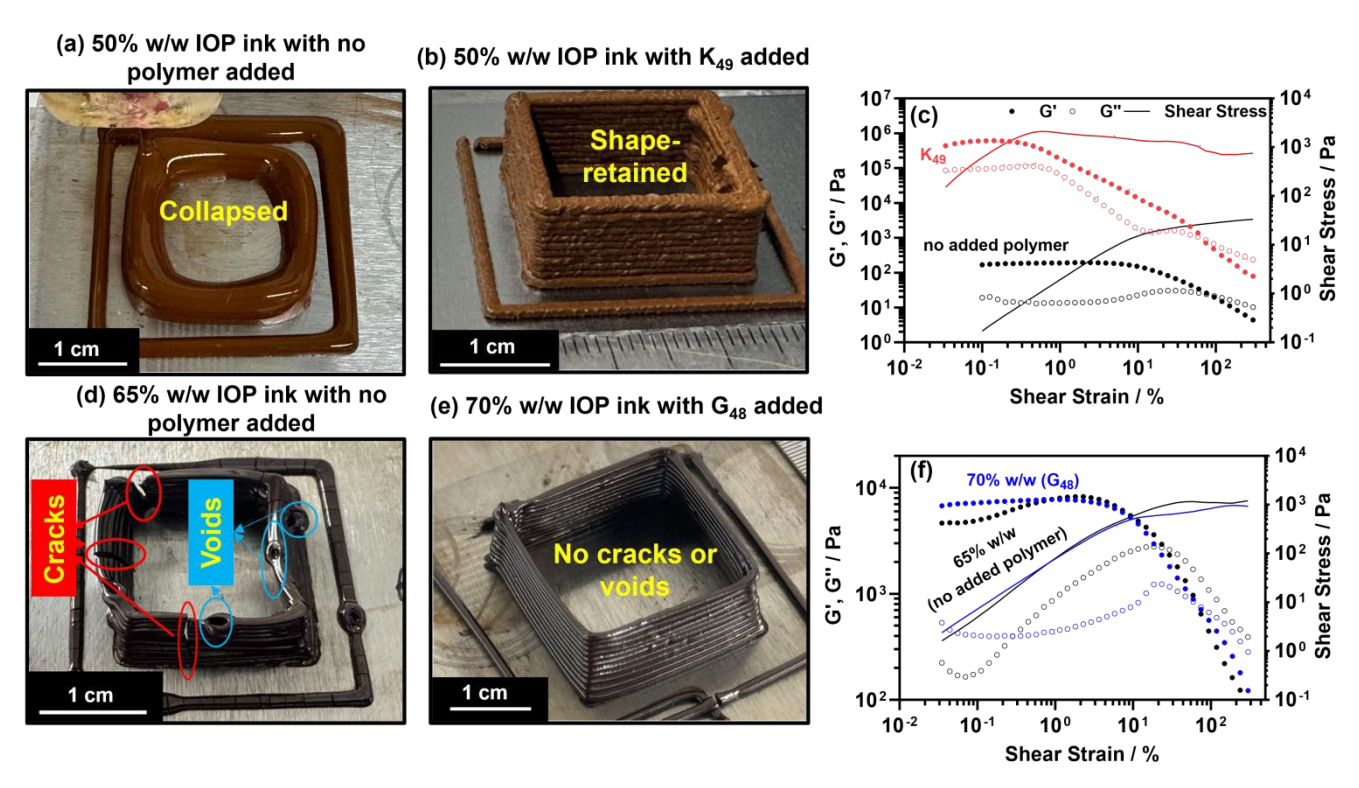


Figure 6. Linking rheology with direct ink writing: Photographs of (a and b) just-printed 11-layer squares using 50% w/w IOP ink with (a) no polymer added at pH 7 and (b) 0.5% w/w K₄₉ added at pH 7; (d and e) printed and dried 11-layer squares using (d) 65% w/w IOP ink with no polymer added at pH 10 and (e) 70% w/w IOP ink with 0.5% w/w G₄₈ added at pH 10; (c and f) Plot of G' (solid dots), G" (hollow dots) and shear stress (solid lines) as a function of shear strain for (c) 50% w/w IOP suspensions with 0.5% w/w K₄₉ added (red) and 50% w/w IOP suspensions with no polymer added to demonstrate how K_{49} thickened the ink at pH 10; (f) 70% w/w IOP suspensions with 0.5% w/w G₄₈ added (blue) and 65% w/w IOP suspensions with no polymer added to show how G₄₈ thinned the ink at pH 10.

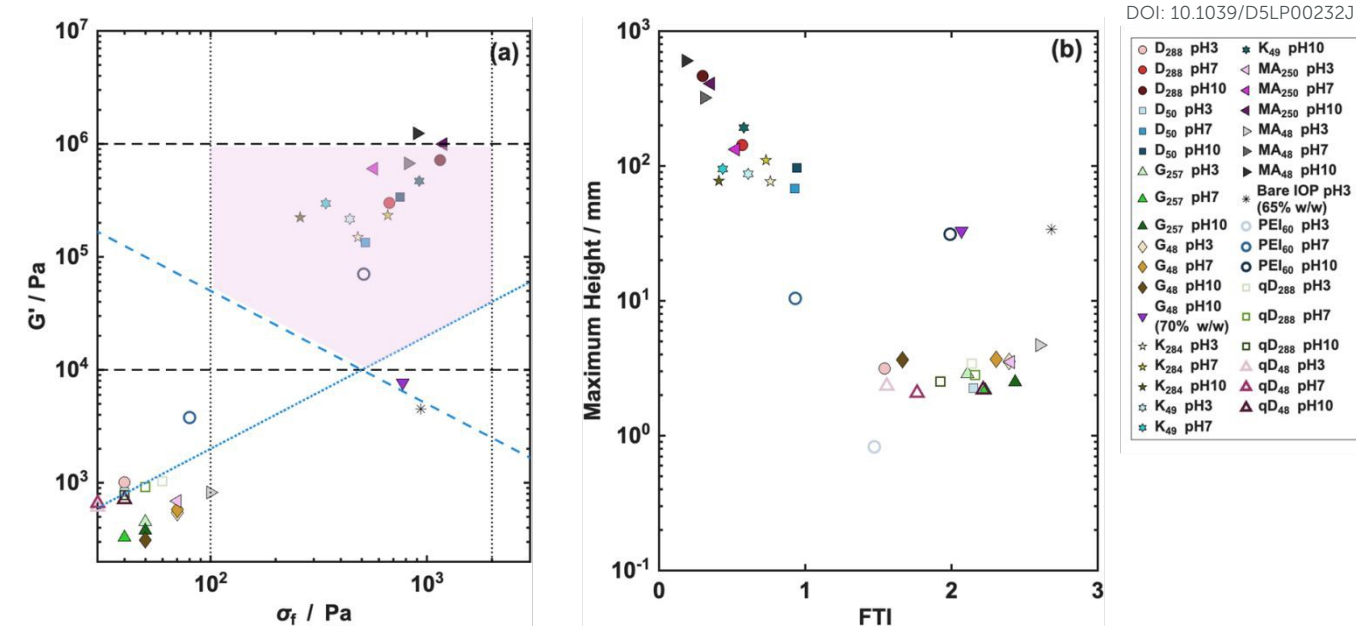


Figure 7. Comparison of IOP suspension rheology against established printability. 51,53,81 (a) storage modulus at LVR (G') vs. flow stress (σ_f) map to demonstrate suspension strength. The two vertical black dotted lines indicate σ_f limits and the two horizontal black dashed lines show G' limits for ceramic DIW. The blue dotted line is the figure of merit (FOM = G'_{LVR}/σ_f = 20) and the blue dashed line indicates Chan's printability criteria. ⁸¹ The pink area is the optimised printability window. (b) The theoretical maximum printable height vs. Flow Transition Index (FTI = σ_f/σ_y), where maximum height = $2\sigma_y/\rho_g$ (where ρ is the ink density and g is gravitational acceleration)⁵¹, demonstrating suspension yield to flow transition, and printing height limitations. The solid loading of suspensions is 50% w/w, except for two samples with different solid loadings indicated in the legend.

Thin-walled squares (dimensions: 20×8×0.84 mm, width× height × wall thickness) were printed onto aluminium substrates using IOP inks formulated with various IOP concentrations, polymer additives and pH (summarised in Table 2). As shown in Figure 6a, the squares printed using 50% w/w IOP ink without added polymer at pH 7 collapsed after printing due to its low G'LVR (340 Pa) and low flow stress (50 Pa). The squares printed using 50% w/w IOP suspension containing 0.5% w/w K₄₉ at pH 7, demonstrated good shape retainability (Figure 6b) due to its increased G'_{LVR} (~ 600 kPa) and shear stress (340 Pa). 50% w/w IOP suspensions containing 0.5% w/w PEI (Figure S20b) or MA48 (Figure S20c) at pH 10 also had good shape retainability thanks to the high G'_{LVR} and shear stress, respectively. However, collapse of the PEI-containing IOP ink at pH 3 was observed (Figure S20a) due to its low G'_{LVR} and shear stress. At the same time, due to the hydrophilic nature of K_{49} , the drying process for objects formulated with this polymer was more uniform and slower,82,83 which resulted in crack-free dried green bodies (Figure S21).

As summarised in Figure 7a and Table 2, K_{49} , D_{50} , PEI and MA_{48} could be used at a suitable pH to improve the ink strength of IOP inks by improving the G'_{LVR} and flow stress. K_{49} was the stand-out from these polymer additives because its thickening effect was not significantly affected by pH, which is promising as these inks could therefore be used under various pH conditions. However, K_{49} was not suitable for high IOP loading inks (> 50% w/w) because adding K_{49} strongly enhanced the ink strength, making the ink challenging to be mixed homogenously and smoothly extruded from the printing nozzle.

Comparing Figure 7a and 7b, while some of the additives enhanced ink strength and maximum printing height, they also decreased the Flow Transition Index (FTI) to < 1. This indicated that the inks became more brittle with an abrupt yield to flow transition. This corresponds to the stress overshot observed for these formulations. Interestingly, the PEI 60K at pH 10 formulation

was an exception as it enhanced the ink strength without making it brittle.

Table 2 Summary of printability and drying conditions of inks in this work

Ink formulation	Printability evaluation	Drying conditions
50% w/w pristine IOP ink at pH 7	Collapsed, poor shape retention	Cracking observed
$50\% \text{ w/w} + 0.5\% \text{ K}_{49} \text{ IOP}$ ink at pH 7	Good shape retention	Crack free
65% w/w pristine IOP ink at pH 10	Collapsed, poor shape retention	Cracking observed
70% w/w IOP + 0.5% G ₄₈ ink at pH 10	Good shape retention	Crack free
50% w/w IOP + 0.5% PEI ink at pH 3	Collapsed, poor shape retention	Cracking observed
50% w/w IOP + 0.5% PEI ink at pH 10	Good shape retention	Crack free
50% w/w IOP + 0.5% MA ₄₈ at pH 10	Good shape retention	Crack free
70% w/w pristine IOP ink at pH 10	Block the nozzle, unprintable	

Printed thin-walled squares using 65% w/w pristine IOPs formed voids during printing due to the non-continuous flow of the ink⁵² and collapsed due to low ink stiffness, with $G'_{LVR} < 10000$ Pa (Figure 6d and Figure 7a). In contrast, adding G_{48} allowed IOP suspensions of 70% w/w to be printed by increasing stiffness and decreasing the flow stress at the same time. Although the G'_{LVR} of G_{48} containing 70% w/w IOP ink was lower than 10000 Pa, which is the lowest limitation in printability map (Figure 7a), this ink still

showed good printability and shape retention. The drying of the ink after extrusion from the nozzle swiftly enhanced the storage modulus, which improved the shape retention of the printed green body. In the meantime, the increased solid loading reduced shrinkage of the green body after drying (Figure 6e). This effect is highly desired for fabricating dense ceramic components, 9,37,84,85 where investigations into the drying behaviour of green bodies printed with different inks and optimised sintering profiles would be required to tailor these inks for different applications.

Conclusions

This article is licensed under a Creative Commons Attribution 3.0 Unported Licence

Open Access Article. Published on 22 10 2025. Downloaded on 2025/11/02 2:35:37.

A library of anionic, cationic, and non-ionic polymers with varying degrees of polymerisation were synthesised via RAFT polymerisation. The effects of these polymer additives on IOP dispersion stability were assessed through zeta potential, DLS for hydrodynamic diameter, DCP for weight-intensity average diameter, and sedimentation tests. Results showed that IOP dispersions without additives were stable at pH 3 but not at pH 7 and 10. Introducing polymers like non-ionic G₄₈ and cationic q-D₄₈, D₅₀, and PEI improved stability at pH 3 via electrosteric and steric repulsion. At pH 7 and 10, MA₄₈ and G₄₈ significantly bolstered stability through electrosteric and steric repulsion, respectively, while other polymers had negligible or adverse effects. Rheological assessment of 50% w/w pristine IOP suspensions, G48 and qD₄₈-containing 50% w/w IOP suspensions indicated a low viscosity, G'_{LVR} and flow stress at all pH vales studied. D₅₀, PEI and MA₄₈-containing IOP suspensions demonstrated low viscosity, G'LVR and flow stress at pH 3. These rheological properties were significantly increased at pH 7 and 10 due to hydrophobic association for D₅₀ and PEI-containing IOP suspensions and polymer network formation for MA₄₈-containing IOP suspensions. K₄₉-containing IOP suspensions consistently showed high viscosity at all pHs and attributed to polymer networks preventing the flow of IOPs. Adding G₄₈, D₅₀, qD₄₈ and PEI reduced the viscosity of 50% w/w IOP suspensions at suitable pHs. However, as IOP loading rose from 50% to 70% w/w, charged polymers q-D $_{\!48}$, D $_{\!50}$, and PEI unexpectedly increased viscosity. Conversely, G_{48} addition consistently lowered the viscosity and flow stress of the suspensions, even at 70% w/w IOP loading.

These polymers played a pivotal role in improving the printability, shape retention and drying behaviour of 3D-printed IOP objects, demonstrated by printing thin-walled squares using various ink formulations onto aluminium substrates. The addition of PEI, K₄₉, or MA_{48} at the appropriate pH notably enhanced the G'_{LVR} , improving shape retention and preventing cracking during drying. Addition of G₄₈ facilitated increased IOP loadings in printable inks from 65% to 70% w/w, yielding low-shrinkage and crack-free green bodies. This multifaceted strategy encompassing polymer synthesis, stability evaluation, rheological characterisation, and 3D printing, underscores the potential of well-defined polymer additives to fine-tune ceramic ink rheology with minimal polymer content (0.5% w/w based on the nanoparticle loading), and lays the groundwork for the development for polymer additives tailored for ceramic ink formulations and advanced 3D printing applications.

Supplementary Information available

Additional experimental methods: schematics of polymer additives synthesis; NMR of polymer additives; GPC of the polymer additives; SEM and TEM of the pristine IOPs; DCP size distribution of IOPs; Rheology data; UV-Vis spectrophotometry data and photograph of 3D printed samples.

Author Information

Corresponding Author

* lee.fielding@manchester.ac.uk

Author Contributions

The manuscript was written through contributions of all authors & all authors have given approval to the final version of the manuscript.

Acknowledgements

The University of Manchester Electron Microscopy Centre is acknowledged for access to electron microscopy facilities. This work was supported by the Henry Royce Institute for Advanced Materials, funded through EPSRC grants EP/R00661X/1, EP/S019367/1, EP/P025021/1, and EP/P025498/1 and the Sustainable Materials Innovation Hub, funded through the European Regional Development Fund OC15R19P. Zhidong Luo would like to acknowledge Dr. Xuzhao Liu for helping with the SEM capture, and Mr. Huize Zheng and Mr. Po-Chun Chiao for assisting with the rheology tests.

References

- K. R. Kunduru, M. Nazarkovsky, S. Farah, R. P. Pawar, A. Basu and A. J. Domb, Nanotechnology for water purification: applications of nanotechnology methods in wastewater treatment, Water Purification, 2017, 33-74.
- H. Zeng, Y. Chen, J. Xu, S. Li, J. Wu, D. Li and J. Zhang, Iron-based materials for activation of periodate in water and wastewater treatment processes: The important role of Fe species, Chemical Engineering Journal, 2024, 482, 148885.
- 3 S. M. Dadfar, K. Roemhild, N. I. Drude, S. von Stillfried, R. Knüchel, F. Kiessling and T. Lammers, Iron oxide nanoparticles: Diagnostic, therapeutic and theranostic applications, Adv Drug Deliv Rev, 2019, 138, 302–325.
- R. Qiao, C. Fu, H. Forgham, I. Javed, X. Huang, J. Zhu, A. K. Whittaker and T. P. Davis, Magnetic iron oxide nanoparticles for brain imaging and drug delivery, Adv Drug Deliv Rev, 2023, 197, 114822.
- 5 E. D. Pereira, F. G. Souza, J. C. C. S. Pinto, R. Cerruti and C. Santana, Synthesis, characterization and drug delivery profile of magnetic PLGA-PEG-PLGA/maghemite nanocomposite, Macromol Symp, 2014, 343, 18-25.
- 6 L. Liu, K. D. T. Ngo and G. Q. Lu, Guideline for paste extrusion 3D printing of slump-free ferrite inductor cores, Ceram Int, 2021, 47, 5803-5811.
- 7 A. Hodaei, O. Akhlaghi, N. Khani, T. Aytas, D. Sezer, B. Tatli, Y. Z. Menceloglu, B. Koc and O. Akbulut, Single Additive Enables 3D Printing of Highly Loaded Iron Oxide Suspensions, ACS Appl Mater Interfaces, 2018, 10, 9873-9881.
- 8 R. L. Fedderwitz, A. E. Hammell, A. B. Lujan, D. Park, J. Fleischer, H. C. Mandujano, E. E. Rodriguez and P. Kofinas, Magnetic Ferrite Nanoparticle Inks for Syringe

- Printable Inductors, ACS Appl Electron Mater, 2024, 6, 3490.
- Z. Luo, Q. Yue, X. Li, Y. Zhu, X. Liu and L. A. Fielding, Polymer-Assisted 3D Printing of Inductor Cores, ACS Appl Mater Interfaces, 2024, 16, 10764–10773.
- N. Travitzky, A. Bonet, B. Dermeik, T. Fey, I. Filbert-Demut, L. Schlier, T. Schlordt and P. Greil, Additive manufacturing of ceramic-based materials, *Adv Eng Mater*, 2014, 16, 729–754.
- Z. Chen, Z. Li, J. Li, C. Liu, C. Lao, Y. Fu, C. Liu, Y. Li,
 P. Wang and Y. He, 3D printing of ceramics: A review, *J Eur Ceram Soc*, 2019, 39, 661–687.
- Y. Yang, D. Cai, Z. Yang, X. Duan, P. He, D. Jia and Y. Zhou, Rheology of organics-free aqueous ceramic suspensions for additive manufacturing of dense silicon nitride ceramics, *Ceram Int*, 2022, **48**, 31941–31951.
- 13 C. de la Torre-Gamarra, M. E. Sotomayor, W. Bucheli, J. M. Amarilla, J. Y. Sanchez, B. Levenfeld and A. Varez, Tape casting manufacturing of thick Li4Ti5O12 ceramic electrodes with high areal capacity for lithium-ion batteries, *J Eur Ceram Soc*, 2021, 41, 1025–1032.
- J. Yang, J. Yu and Y. Huang, Recent developments in gelcasting of ceramics, *J Eur Ceram Soc*, 2011, 31, 2569– 2591.
- J. E. Kanyo, S. Schafföner, R. S. Uwanyuze and K. S. Leary, An overview of ceramic molds for investment casting of nickel superalloys, *J Eur Ceram Soc*, 2020, 40, 4955–4973.
- 16 H. Le Ferrand, Magnetic slip casting for dense and textured ceramics: A review of current achievements and issues, *J Eur Ceram Soc*, 2021, **41**, 24–37.
- M. Suárez, L. A. Díaz, J. F. Bartolomé, A. Borrell, S. López-Esteban, R. Torrecillas, J. S. Moya and A. Fernández, Null-thermal expansion coefficient LAS-nSiC composite by slip-casting, *J Eur Ceram Soc*, 2022, 42, 7228–7236.
- H. wei Li, Y. peng Zhao, G. qing Chen, M. hao Li, X. song Fu and W. long Zhou, Synergy of low-and high-density polyethylene in a binder system for powder injection molding of SiC ceramics, *Ceram Int*, 2022, 48, 25513– 25520.
- 19 R. Wick-Joliat, M. Tschamper, R. Kontic and D. Penner, Water-soluble sacrificial 3D printed molds for fast prototyping in ceramic injection molding, *Addit Manuf*, 2021, **48**, 102408.
- Y. Lakhdar, C. Tuck, J. Binner, A. Terry and R. Goodridge, Additive manufacturing of advanced ceramic materials, *Prog Mater Sci*, 2021, 116, 100736.
- 21 C. E. Cipriani, D. A. Dornbusch, S. L. Vivod and E. B. Pentzer, Direct ink writing of polyimide aerogels for

battery thermal mitigation, *RSC Applied Polymers*, 2023, **2**, 71–86.

View Article Online

- 22 L. del-Mazo-Barbara and M.-P. Ginebra, Rheological characterisation of ceramic inks for 3D direct ink writing: A review, *J Eur Ceram Soc*, 2021, 41, 18–33.
- M. A. S. R. Saadi, A. Maguire, N. T. Pottackal, M. S. H. Thakur, M. M. Ikram, A. J. Hart, P. M. Ajayan and M. M. Rahman, Direct Ink Writing: A 3D Printing Technology for Diverse Materials, *Advanced Materials*, 2022, 34, 1–57
- A. M'Barki, L. Bocquet and A. Stevenson, Linking Rheology and Printability for Dense and Strong Ceramics by Direct Ink Writing, *Sci Rep*, 2017, **7**, 6017.
- V. G. Rocha, E. Saiz, I. S. Tirichenko and E. García-Tuñón, Direct ink writing advances in multi-material structures for a sustainable future, *J Mater Chem A Mater*, 2020, **8**, 15646–15657.
- 26 S. N. Lak, C.-M. Hsieh, L. AlMahbobi, Y. Wang, A. Chakraborty, C. Yu and E. B. Pentzer, Printing Composites with Salt Hydrate Phase Change Materials for Thermal Energy Storage, ACS Applied Engineering Materials, 2023, 1, 2279–2287.
- 27 R. H. Ewoldt, A. E. Hosoi and G. H. McKinley, New measures for characterizing nonlinear viscoelasticity in large amplitude oscillatory shear, *J Rheol (N Y N Y)*, 2008, **52**, 1427–1458.
- 28 R. Agrawal and E. García-Tuñón, Interplay between yielding, 'recovery', and strength of yield stress fluids for direct ink writing: new insights from oscillatory rheology, Soft Matter, 2024, 20, 7429–7447.
- Q. Yue, Z. Luo, X. Li and L. A. Fielding, 3D printable, thermo-responsive, self-healing, graphene oxide containing self-assembled hydrogels formed from block copolymer wormlike micelles, *Soft Matter*, 2023, **19**, 6513–6524.
- 30 E. L. Jones, Z. Luo, R. Agrawal, S. Flynn, M. Carr, W. Sharratt and E. García-Tuñón, Designing yield stress fluids for advanced materials processing using derivatives of pH-responsive branched co-polymer surfactants, *Soft Matter*, 2025, **21**, 4822–4838.
- 31 B. G. Compton and J. A. Lewis, 3D-printing of lightweight cellular composites, *Advanced Materials*, 2014, **26**, 5930–5935.
- G. Siqueira, D. Kokkinis, R. Libanori, M. K. Hausmann, A. S. Gladman, A. Neels, P. Tingaut, T. Zimmermann, J. A. Lewis and A. R. Studart, Cellulose Nanocrystal Inks for 3D Printing of Textured Cellular Architectures, *Adv Funct Mater*, 2017, 27, 1604619.
- E. García-Tuñón, E. Feilden, H. Zheng, E. D'Elia, A. Leong and E. Saiz, Graphene Oxide: An All-in-One

- Processing Additive for 3D Printing, ACS Appl Mater Interfaces, 2017, **9**, 32977–32989.
- Y. Yang, Z. Yang, X. Duan, P. He, D. Cai, D. Jia and Y. Zhou, Large-size Si3N4 ceramic fabricated by additive manufacturing using long-term stable hydrogel-based suspensions, *Addit Manuf*, 2023, 69, 103534.
- Q. Yue, S. Wang, S. T. Jones and L. A. Fielding, Multifunctional Self-Assembled Block Copolymer/Iron Oxide Nanocomposite Hydrogels Formed from Wormlike Micelles, ACS Appl Mater Interfaces, 2024, 16, 21197– 21209.
- Y. Lakhdar, C. Tuck, A. Terry and R. Goodridge, Dispersion and stability of colloidal boron carbide suspensions, *Ceram Int*, 2020, 46, 27957–27966.
- 37 I. L. de Camargo, M. M. Morais, C. A. Fortulan and M. C. Branciforti, A review on the rheological behavior and formulations of ceramic suspensions for vat photopolymerization, *Ceram Int*, 2021, 47, 11906–11921.
- M. Yaghtin, A. Yaghtin, Z. Tang and T. Troczynski, Improving the rheological and stability characteristics of highly concentrated aqueous yttria stabilized zirconia slurries, *Ceram Int*, 2020, 46, 26991–26999.
- Z. Goharibajestani, O. Akhlaghi, C. Akaoglu, F. Afghah, N. Khani, A. Hodaei, B. Koc and O. Akbulut, Incorporating Steric Hindrance into the Additive Design Enables a Robust Formulation of Alumina Ink for Extrusion-based 3D Printing, ACS Appl Polym Mater, 2019, 1, 3279–3285.
- 40 A. Dörr, A. Sadiki and A. Mehdizadeh, A discrete model for the apparent viscosity of polydisperse suspensions including maximum packing fraction, *J Rheol (N Y N Y)*, 2013, **57**, 743–765.
- G. Ding, R. He, K. Zhang, M. Xia, C. Feng and D. Fang, Dispersion and stability of SiC ceramic slurry for stereolithography, *Ceram Int*, 2020, **46**, 4720–4729.
- 42 X. Xu, J. Yang, W. Jonhson, Y. Wang, A. Suwardi, J. Ding, C. Guan and D. Zhang, Additive manufacturing solidification methodologies for ink formulation, *Addit Manuf*, 2022, 56, 102939.
- 43 H. Wang, C. Chen, F. Yang, Y. Shao and Z. Guo, Direct ink writing of metal parts with curing by UV light irradiation, *Mater Today Commun*, 2021, 26, 102037.
- M. Li, S. Huang, E. Willems, J. Soete, M. Inokoshi, B. Van Meerbeek, J. Vleugels and F. Zhang, UV-Curing Assisted Direct Ink Writing of Dense, Crack-Free, and High-Performance Zirconia-Based Composites With Aligned Alumina Platelets, Adv Mater, 2024, 36, 2306764.
- 45 C. M. Clarkson, C. Wyckoff, M. J. S. Parvulescu, L. M. Rueschhoff and M. B. Dickerson, UV-assisted direct ink

- DOI: 10.1039/D5LP00232J writing of Si3N4/SiC preceramic polymer suspensions, *J Eur Ceram Soc*, 2022, **42**, 3374–3382.
- 46 H. Watanabe and J. Seto, Specific Acidities of the Surface Hydroxyl Groups on Maghemite, *Bull Chem Soc Jpn*, 1993, 66, 395–399.
- 47 S. Wan, Y. Zheng, Y. Liu, H. Yan and K. Liu, Fe3O4 Nanoparticles coated with homopolymers of glycerol mono(meth)acrylate and their block copolymers, *J Mater Chem*, 2005, **15**, 3424–3430.
- 48 S. Yu and C. M. Chow, Carboxyl group (-CO2H) functionalized ferrimagnetic iron oxide nanoparticles for potential bio-applications, *J Mater Chem*, 2004, **14**, 2781–2786.
- 49 C. Liang, B. Wang, J. Chen, Y. Huang, T. Fang, Y. Wang and B. Liao, The effect of acrylamides copolymers on the stability and rheological properties of yellow iron oxide dispersion, *Colloids Surf A Physicochem Eng Asp*, 2017, 513, 136–145.
- 50 M. J. McGuire, J. Addai-Mensah and K. E. Bremmell, The effect of polymer structure type, pH and shear on the interfacial chemistry, rheology and dewaterability of model iron oxide dispersions, *Colloids Surf A Physicochem Eng Asp*, 2006, **275**, 153–160.
- 51 P. Wei, C. Cipriani, C. M. Hsieh, K. Kamani, S. Rogers and E. Pentzer, Go with the flow: Rheological requirements for direct ink write printability, *J Appl Phys*, 2023, **134**, 1–3.
- 52 E. García-Tuñón, R. Agrawal, B. Ling and D. J. C. Dennis, Fourier-transform rheology and printability maps of complex fluids for three-dimensional printing, *Physics of Fluids*, 2023, 35, 017113.
- Z. L. Li, S. Zhou, E. Saiz and R. Malik, Ink formulation in direct ink writing of ceramics: A meta-analysis, *J Eur Ceram Soc*, 2024, 44, 6777–6796.
- J. M. Berg, A. Romoser, N. Banerjee, R. Zebda and C. M. Sayes, The relationship between pH and zeta potential of ~ 30 nm metal oxide nanoparticle suspensions relevant to in vitro toxicological evaluations, *Nanotoxicology*, 2009, 3, 276–283.
- J. A. Lewis, Colloidal Processing of Ceramics, *Journal of the American Ceramic Society*, 2000, **83**, 2341–2359.
- L. A. Fielding, C. T. Hendley, E. Asenath-Smith, L. A. Estroff and S. P. Armes, Rationally designed anionic diblock copolymer worm gels are useful model systems for calcite occlusion studies, *Polym Chem*, 2019, 10, 5131–5141.
- 57 S. Laurent, D. Forge, M. Port, A. Roch, C. Robic, L. Vander Elst and R. N. Muller, Magnetic Iron Oxide Nanoparticles: Synthesis, Stabilization, Vectorization, Physicochemical Characterizations, and Biological Applications, Chem Rev, 2010, 110, 2574–2574.

This article is licensed under a Creative Commons Attribution 3.0 Unported Licence

Open Access Article. Published on 22 10 2025. Downloaded on 2025/11/02 2:35:37.

- V. Bütün, S. P. Armes and N. C. Billingham, Synthesis and aqueous solution properties of near-monodisperse tertiary amine methacrylate homopolymers and diblock copolymers, *Polymer (Guildf)*, 2001, 42, 5993–6008.
- 60 P. Liu, B. Yu, B. Peng, X. Sun, W. Chen, S. Yang, R. Lu, J. Zhang, D. Yang, H. Cui, P. Yang and Y. Ning, Spatially Controlled Distribution of Copolymer Nanoparticles within Calcite Crystals Enabled by Engineering Surface Chemistry, Cryst Growth Des, 2025, 25, 2031–2042.
- D. B. Genovese, Shear rheology of hard-sphere, dispersed, and aggregated suspensions, and filler-matrix composites, *Adv Colloid Interface Sci*, 2012, **171–172**, 1–16.
- 62 X. Li, Z. Luo and L. A. Fielding, Pyrene-Decorated Thermally Responsive Luminescent Nanoparticles: The Effect of Copolymer Micelle Morphology, *Macromolecules*, 2025, 58, 5995–6004.
- 63 S. A. Vshivkov, T. S. Soliman, E. S. Kluzhin and A. A. Kapitanov, Structure of poly(acrylic acid), poly(methacrylic acid) and gelatin solutions, *J Mol Liq*, 2019, 294, 111551.
- 64 C. Chassenieux, T. Nicolai and L. Benyahia, Rheology of associative polymer solutions, *Curr Opin Colloid Interface Sci*, 2011, **16**, 18–26.
- 65 R. H. Colby, Structure and linear viscoelasticity of flexible polymer solutions: comparison of polyelectrolyte and neutral polymer solutions, *Rheol Acta*, 2010, **49**, 425–442.
- J. F. Morris, Shear Thickening of Concentrated Suspensions: Recent Developments and Relation to Other Phenomena, Annu Rev Fluid Mech, 2020, 52, 121–144.
- V. Tomeckova and J. W. Halloran, Flow behavior of polymerizable ceramic suspensions as function of ceramic volume fraction and temperature, *J Eur Ceram Soc*, 2011, **31**, 2535–2542.
- 68 S. C. Hauswirth, C. A. Bowers, C. P. Fowler, P. B. Schultz, A. D. Hauswirth, T. Weigand and C. T. Miller, Modeling cross model non-Newtonian fluid flow in porous media, *J Contam Hydrol*, 2020, 235, 103708.
- 69 R. Agrawal, P. T. Spicer and E. García-Tuñón, Connecting bulk rheology, structural transitions and heterogeneous flow in Pluronic F127 micellar cubic liquid crystals using rheo-microscopy, *J Colloid Interface Sci*, 2025, 699, 138226.
- 70 A. Lele, A. Shedge, M. Badiger, P. Wadgaonkar and C. Chassenieux, Abrupt Shear Thickening of Aqueous

- Solutions of Hydrophobically Modified Poly(N , N '-dimethylacrylamide- co -acrylic acid), *Macromolecules*, 2010, **43**, 10055–10063.
- 71 Y. Tan, W. Zhang, Y. Li, Y. Xia and K. Sui, Grafting of multi-sensitive PDMAEMA brushes onto carbon nanotubes by ATNRC: tunable thickening/thinning and self-assembly behaviors in aqueous solutions, *RSC Adv*, 2016, **6**, 92305–92315.
- 72 K. A. Curtis, D. Miller, P. Millard, S. Basu, F. Horkay and P. L. Chandran, Unusual Salt and pH Induced Changes in Polyethylenimine Solutions, *PLoS One*, 2016, 11, 0158147.
- 73 S. P. Wen, J. G. Saunders and L. A. Fielding, Investigating the influence of solvent quality on RAFT-mediated PISA of sulfonate-functional diblock copolymer nanoparticles, *Polym Chem*, 2020, **11**, 3416–3426.
- R. Du and L. A. Fielding, Preparation of polymer nanoparticle-based complex coacervate hydrogels using polymerisation-induced self-assembly derived nanogels, *Soft Matter*, 2023, **19**, 2074–2081.
- 75 R. Du and L. A. Fielding, pH-Responsive Nanogels Generated by Polymerization-Induced Self-Assembly of a Succinate-Functional Monomer, *Macromolecules*, 2024, 57, 3496–3501.
- W. Chen, P. Liu, X. Sun, B. Xiong, H. Cui, Z. Zhao and Y. Ning, Spatioselective Occlusion of Copolymer Nanoparticles within Calcite Crystals Generates Organic-Inorganic Hybrid Materials with Controlled Internal Structures, Angewandte Chemie, 2024, 136, e202410908.
- 77 X. Cheng, T. Miao, Y. Ma, X. Zhu, W. Zhang and X. Zhu, Controlling the Multiple Chiroptical Inversion in Biphasic Liquid-Crystalline Polymers, *Angewandte Chemie International Edition*, 2021, **60**, 24430–24436.
- 78 S. M. North and S. P. Armes, Aqueous solution behavior of stimulus-responsive poly(methacrylic acid)-poly(2-hydroxypropyl methacrylate) diblock copolymer nanoparticles, *Polym Chem*, 2020, **11**, 2147–2156.
- M. Semsarilar, V. Ladmiral, A. Blanazs and S. P. Armes, Cationic polyelectrolyte-stabilized nanoparticles via RAFT aqueous dispersion polymerization, *Langmuir*, 2013, 29, 7416–7424.
- A. P. R. Eberle and L. Porcar, Flow-SANS and Rheo-SANS applied to soft matter, *Curr Opin Colloid Interface Sci*, 2012, **17**, 33–43.
- 81 S. S. L. Chan, M. L. Sesso and G. V. Franks, Direct ink writing of hierarchical porous alumina-stabilized emulsions: Rheology and printability, *Journal of the American Ceramic Society*, 2020, **103**, 5554–5566.
- K. Huang, G. Liu, J. Shen, Z. Chu, H. Zhou, X. Gu, W. Jin and N. Xu, High-Efficiency Water-Transport Channels using the Synergistic Effect of a Hydrophilic

83 D. Rinaldi, T. Hamaide, C. Graillat, F. D'Agosto, R. Spitz, S. Georges, M. Mosquet and P. Maitrasse, RAFT copolymerization of methacrylic acid and poly(ethylene glycol) methyl ether methacrylate in the presence of a hydrophobic chain transfer agent in organic solution and in water, J Polym Sci A Polym Chem, 2009, 47, 3045-3055.

This article is licensed under a Creative Commons Attribution 3.0 Unported Licence.

Open Access Article. Published on 22 10 2025. Downloaded on 2025/11/02 2:35:37.

- DOI: 10.1039/D5LP00232J E. Peng, X. Wei, U. Garbe, D. Yu, B. Edouard, A. Liu and 84 J. Ding, Robocasting of dense yttria-stabilized zirconia structures, J Mater Sci, 2018, 53, 247-273.
- 85 L. Rueschhoff, W. Costakis, M. Michie, J. Youngblood and R. Trice, Additive Manufacturing of Dense Ceramic Parts via Direct Ink Writing of Aqueous Alumina Suspensions, Int J Appl Ceram Technol, 2016, 13, 821-830.

Open Access Article. Published on 22 10 2025. Downloaded on 2025/11/02 2:35:37.

This article is licensed under a Creative Commons Attribution 3.0 Unported Licence

View Article Online DOI: 10.1039/D5LP00232J

Data Availability Statement for:

Enhancement of high concentration aqueous iron oxide nanoparticle ink printability through well-defined polymer additives

Zhidong Luo, a,b,c Xueyuan Li a,b and Lee A. Fielding*a,b

- a. Department of Materials, School of Natural Sciences, University of Manchester, Oxford Road, Manchester, M13 9PL, U.K.
- b. Henry Royce Institute, The University of Manchester, Oxford Road, Manchester, M13 9PL, U.K.
- c. School of Engineering, The University of Liverpool, Liverpool L69 3BX, U.K.
 - * Corresponding author: lee.fielding@manchester.ac.uk

The data supporting this article have been included as part of the Supplementary Information.